

# Non-invasive optical neuromonitoring of the temperature-dependence of cerebral oxygen metabolism during deep hypothermic cardiopulmonary bypass in neonatal swine

Journal of Cerebral Blood Flow & Metabolism  
0(00) 1–17  
© Author(s) 2018  
Article reuse guidelines:  
sagepub.com/journals-permissions  
DOI: 10.1177/0271678X18809828  
journals.sagepub.com/home/jcbfm



Tiffany S Ko<sup>1,2,3</sup>, Constantine D Mavroudis<sup>4</sup>, Wesley B Baker<sup>3</sup>, Vincent C Morano<sup>2</sup>, Kobina Mensah-Brown<sup>3</sup>, Timothy W Boorady<sup>3</sup>, Alexander L Schmidt<sup>5</sup>, Jennifer M Lynch<sup>6</sup>, David R Busch<sup>7,8</sup>, Javier Gentile<sup>9</sup>, George Bratinov<sup>6</sup>, Yuxi Lin<sup>6</sup>, Sejin Jeong<sup>6</sup>, Richard W Melchior<sup>10</sup>, Tami M Rosenthal<sup>10</sup>, Brandon C Shade<sup>10</sup>, Kellie L Schiavo<sup>10</sup>, Rui Xiao<sup>11</sup>, J William Gaynor<sup>9</sup>, Arjun G Yodh<sup>2</sup>, Todd J Kilbaugh<sup>6</sup> and Daniel J Licht<sup>3</sup>

## Abstract

Management of deep hypothermic (DH) cardiopulmonary bypass (CPB), a critical neuroprotective strategy, currently relies on non-invasive temperature to guide cerebral metabolic suppression during complex cardiac surgery in neonates. Considerable inter-subject variability in temperature response and residual metabolism may contribute to the persisting risk for postoperative neurological injury. To characterize and mitigate this variability, we assess the sufficiency of conventional nasopharyngeal temperature (NPT) guidance, and in the process, validate combined non-invasive frequency-domain diffuse optical spectroscopy (FD-DOS) and diffuse correlation spectroscopy (DCS) for direct measurement of cerebral metabolic rate of oxygen ( $CMRO_2$ ). During CPB,  $n=8$  neonatal swine underwent cooling from normothermia to 18°C, sustained DH perfusion for 40 min, and then rewarming to simulate cardiac surgery. Continuous non-invasive and invasive measurements of intracranial temperature (ICT) and  $CMRO_2$  were acquired. Significant hysteresis ( $p < 0.001$ ) between cooling and rewarming periods in the NPT versus ICT and NPT versus  $CMRO_2$  relationships were found. Resolution of this hysteresis in the ICT versus  $CMRO_2$  relationship identified a crucial insufficiency of conventional NPT guidance. Non-invasive  $CMRO_2$  temperature coefficients with respect to NPT ( $Q_{10} = 2.0$ ) and ICT ( $Q_{10} = 2.5$ ) are consistent with previous reports and provide further validation of FD-DOS/DCS  $CMRO_2$  monitoring during DH CPB to optimize management.

<sup>1</sup>Department of Bioengineering, University of Pennsylvania, Philadelphia, PA, USA

<sup>2</sup>Department of Physics and Astronomy, University of Pennsylvania, Philadelphia, PA, USA

<sup>3</sup>Division of Neurology, Children's Hospital of Philadelphia, Philadelphia, PA, USA

<sup>4</sup>Division of Cardiovascular Surgery, Department of Surgery, Hospital of the University of Pennsylvania, Philadelphia, PA, USA

<sup>5</sup>Department of Biology, James Madison University, Harrisonburg, VA, USA

<sup>6</sup>Department of Anesthesiology and Critical Care Medicine, Children's Hospital of Philadelphia, Philadelphia, PA, USA

<sup>7</sup>Department of Anesthesiology & Pain Management, University of Texas Southwestern, Dallas, TX, USA

<sup>8</sup>Department of Neurology & Neurotherapeutics, University of Texas Southwestern, Dallas, TX, USA

<sup>9</sup>Division of Cardiothoracic Surgery, Children's Hospital of Philadelphia, Philadelphia, PA, USA

<sup>10</sup>Department of Perfusion Services, Cardiac Center, Children's Hospital of Philadelphia, Philadelphia, PA, USA

<sup>11</sup>Department of Pediatrics, Division of Biostatistics, Children's Hospital of Philadelphia, Philadelphia, PA, USA

## Corresponding author:

Tiffany S Ko, Laboratory for the Research on the Structure of Matter, University of Pennsylvania, 3231 Walnut St., Philadelphia, PA 19104, USA.  
Email: tiko@seas.upenn.edu

## Keywords

Cerebral oxygen metabolism, cardiopulmonary bypass, diffuse correlation spectroscopy, diffuse optical spectroscopy, deep hypothermia

Received 12 May 2018; Revised 19 September 2018; Accepted 20 September 2018

## Introduction

Deep hypothermia (DH) is an important neuroprotective therapy used during cardiopulmonary bypass (CPB) in an attempt to mitigate hypoxic–ischemic brain injury by suppressing cellular metabolic demand in neonates with congenital heart disease during complex cardiac repairs.<sup>1</sup> Over the last two decades, survival rates for these children have substantially improved<sup>2</sup>; however, the incidence of neurological injury has remained constant and, in some cases, has resulted in developmental delays and lifelong neurological deficits.<sup>3</sup> Despite widespread use of DH CPB, uncertainty predominates regarding optimal temperature management due to hitherto poorly defined individual cerebral metabolic responses to hypothermia.

Real-time neuromonitoring is needed to address a key challenge for DH protocols by confirming, on a patient-by-patient basis, that the suppression of metabolism is sufficient to prevent adverse neurological sequelae during procedural cerebral ischemia.<sup>1,4–6</sup> Decreased cerebral blood flow (CBF), oxygen extraction, and metabolism in response to DH have been widely demonstrated, but significant inter-subject variability in temperature-response has also been observed.<sup>7</sup> Specifically, the use and value of conventional core temperature guidance for assessment of the adequacy of metabolic suppression during DH have been questioned.<sup>8–12</sup> Systematic study of core temperature, brain temperature, and residual cerebral metabolism as neurological risk factors is needed. Such studies are hindered by a lack of noninvasive, cerebral metabolic monitoring tools suitable for the operative environment. If this limitation can be ameliorated, then assessment of current neuroprotection strategies, and development of new personalized strategies to optimize neurological outcomes, should be possible for these at-risk children.

Multimodal neuromonitoring, including clinical continuous-wave near-infrared spectroscopy (CW NIRS) for cerebral oxygen saturation and transcranial Doppler ultrasound (TCD) for CBF-velocity, has shown evidence of improving post-operative neurological complications.<sup>13</sup> The quantitative uncertainty of CW NIRS and the logistical difficulty of employing and interpreting TCD in the operating room have prevented their combined use for routine metabolic monitoring and likely impacted efficacy of goal-directed

therapy.<sup>14</sup> By contrast, the combination of frequency- or time-domain diffuse optical spectroscopy (FD-DOS, TD-DOS), to measure *absolute* cerebral tissue oxygen saturation (StO<sub>2</sub>, %), with diffuse correlation spectroscopy (DCS) to measure CBF, enables a compact, all-optical method for continuous non-invasive monitoring of cerebral metabolism. This approach has been demonstrated in vulnerable pediatric populations outside the operating room.<sup>15–28</sup> Although recent work has established intraoperative feasibility for some of this technology,<sup>20,29</sup> non-invasive diffuse optical measurements of CBF and metabolism have never been validated against invasive monitoring during the profound physiologic and temperature changes induced by DH CPB and subsequent rewarming.

Here we carry out an observational study of concurrent conventional monitoring of nasopharyngeal temperature (NPT) alongside invasive intracranial temperature (ICT) and invasive and non-invasive (i.e. diffuse optical) measurements of cerebral oxygen metabolism during a simulated cardiac surgical procedure using DH CPB with subsequent rewarming in neonatal swine. The sufficiency of NPT guidance is examined with respect to ICT, and the temperature-dependence of cerebral oxygen metabolism is assessed with respect to both modalities using high temporal resolution *in vivo* sampling methods. Non-invasive diffuse optical measurements are compared directly with invasive measurements, and similarities and differences of measured parameters are identified and understood.

## Methods

Neonatal, female Yorkshire swine ( $n=8$ , 6–10 days old, 3–5 kg) were continuously monitored during CPB from induction of DH through recovery to normothermia. All procedures were approved by the CHOP Institutional Animal Care and Use Committee, performed in strict accordance with the NIH Guide for the Care and Use of Laboratory Animals, and reported according to the ARRIVE guidelines (<https://www.nc3rs.org.uk/arrive-guidelines>).

### Selection of animal model

Pediatric large-animal model studies describing *CMRO*<sub>2</sub> temperature-dependence during DH CPB have been reported in dogs<sup>30</sup> and pigs using sparse

sampling methods.<sup>12,31–36</sup> The neonatal swine model offers comparable anatomical size and cortical maturation with the human neonate, as well as excellent intersection of DH CPB and diffuse optical neuro-monitoring literature.<sup>23,37–39</sup>

### Neuromonitoring

Non-invasive and invasive neuromonitoring were placed and secured following anesthetic induction and intubation as detailed in Supplementary Materials, Section S.1.<sup>40</sup> Continuous non-invasive measurements comprised NPT (°C), for guidance of hypothermic therapy, and frequency-domain diffuse optical spectroscopy (FD-DOS) and DCS. NPT, which has been found to be a close surrogate of parenchymal brain temperature,<sup>41</sup> was measured using a thermistor (Level 1 Thermistor GP Probe, Smith Medical) inserted 5 cm to the mid-nasopharynx and sutured into place. FD-DOS/DCS measurements were acquired in the left frontal cortex via an optical probe sutured to the left forehead (Figure 1). Continuous invasive neuromonitoring was performed symmetrically on the contralateral hemisphere through small burr holes made over the right frontal cortex (10 mm paramedian, 10 mm anterior to the coronal suture; Figure 1). Subcortical intracranial oxygen tension ( $P_{btO_2}$ , mmHg) and cortical ICT (°C) were measured 15 mm and 5 mm, respectively, below the cortical surface (Licox CC1-P1, Integra LifeSciences) near the junction of grey and subcortical white matter. Relative cortical cerebral blood flow (rCBF LD, %) was measured with a laser Doppler probe (PeriFlux 5000, Perimed Inc.) secured to the dura matter. A double lumen, 4F central venous catheter was placed in the superior vena cava and advanced into the internal jugular bulb for invasive discontinuous sampling of cerebral venous drainage.

### DH protocol

Protocols for institution of DH CPB are detailed in Supplementary Materials, Section S.1 and closely mirrored clinical practice at our institution (Figure 2). Subjects were stabilized on CPB at normothermia (NPT=37°C) and baseline measurements acquired for 5 min. Guided by NPT, subjects were then cooled at a target rate of 1°C per minute to 18°C in order to characterize cerebral metabolism across the full range of temperatures currently used in neonates.<sup>42,43</sup> Subjects were then maintained on continuous DH perfusion for 40 min. Rewarming to normothermia occurred at a target rate of 1°C per minute. Invasive arterial and venous blood gas sampling (0.3 cc of blood per draw from the bypass arterial outflow and jugular bulb, respectively) occurred at the start of cooling (i.e.

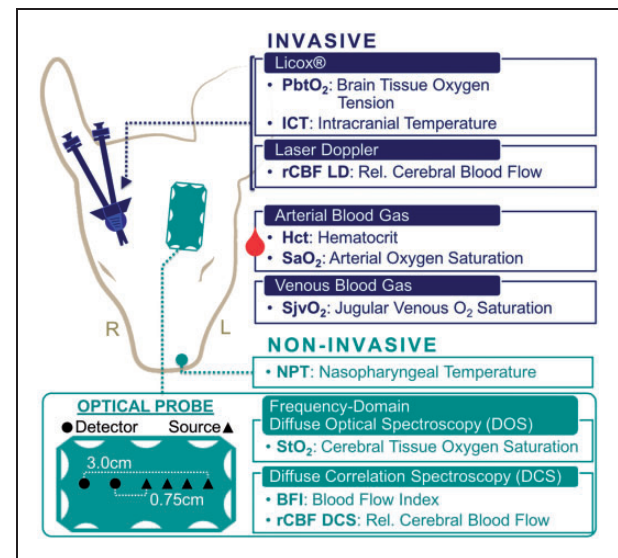


**Figure 1.** Neuromonitoring – Head placement of *non-invasive* (green; left hemisphere) and *invasive* (blue; right hemisphere) neuromonitoring technologies. A diagram showing details about the FD-DOS/DCS optical probe is given on the lower left (source positions, triangles; detector positions, circles).

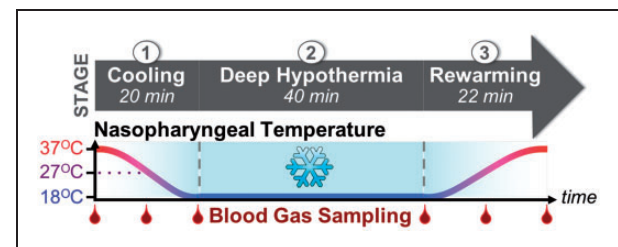


**Figure 2.** Temperature and blood gas sampling protocol – Each subject underwent three stages of treatment: (1) Induction of deep hypothermia (“Cooling”); (2) 40 min of continuous cold perfusion (“Deep Hypothermia”); (3) Recovery from deep hypothermia (“Rewarming”). Arterial and jugular venous blood gas sampling was performed at multiple time-points indicated by red droplets along the time-axis.

baseline, 37°C), midpoint of cooling (27°C), end of cooling (18°C), start of rewarming (18°C), midpoint of rewarming (27°C) and end of rewarming (37°C; Figure 2). Immediate analysis was facilitated through a point-of-care blood gas analyzer (GEM 3000, Instrumentation Laboratory). Blood pH was optimized by pH-stat management during cooling. During rewarming and while normothermic, blood pH was optimized by alpha-stat.

### Diffuse optical techniques

*Frequency-domain diffuse optical spectroscopy.* Multi-distance FD-DOS was used to continuously measure

cerebral tissue oxygen saturation ( $StO_2$ , %) and oxygen extraction fraction ( $OEF$ ). FD-DOS employs radio-frequency intensity-modulated near-infrared light to quantify wavelength-dependent absorption and scattering properties of tissue.<sup>44-46</sup>

A customized, commercial instrument (Imagent, ISS Inc.), equipped with four 690, 725, 785, and 830 nm intensity-modulated (110 MHz) diode laser sources and two photomultiplier tube detectors, was coupled to the fiberoptic probe; source-detector separations ranged from 0.75 cm to 3 cm (Figure 1, lower left). For each subject, the source- and detector-fiber coupling coefficients to the tissue were estimated using a phantom-calibration approach<sup>47</sup> and used to correct continuous (10 Hz) AC intensity and phase data. Using a multi-distance linear fitting method, absolute absorption and scattering coefficients were calculated for each wavelength from these data. Coefficients were excluded if the linear fit Pearson correlation coefficient was  $<0.95$ , and the data-point excluded if more than one of the four scattering or absorption coefficients were excluded. Assuming a cerebral water volume fraction of 75%,<sup>48</sup> the absolute cerebral tissue concentration of oxy-hemoglobin ( $[HbO_2]$ ,  $\mu\text{mol/L}$ ) and deoxy-hemoglobin ( $[Hb]$ ,  $\mu\text{mol/L}$ ) was quantified from the absorption coefficient<sup>45</sup> and  $StO_2$  calculated as

$$StO_2(\%) = \frac{[HbO_2]}{[Hb] + [HbO_2]} \quad (1)$$

Importantly, the FD-DOS technique directly measures the tissue scattering coefficient and eliminates optical absorption measurement errors introduced by physiologic shifts in optical scattering,<sup>49,50</sup> a parameter which cannot be determined by commercial CW NIRS.

**DCS.** DCS is a photon correlation technique that derives a CBF index (BFI,  $\text{cm}^2/\text{s}$ ) from quantification of the rapid speckle intensity fluctuations of multiply scattered coherent near-infrared light induced by red blood cell motion.<sup>38,51,52</sup> DCS measurements were made using a source-detector separation of 2.5 cm, wherein the detected light fields were sensitive to blood flow at an average depth of 1 cm below the scalp surface.<sup>53</sup>

The DCS light source was a continuous-wave, long-coherence length ( $>10\text{ m}$ ), 785 nm laser (RCL-080-785S, CrystaLaser, Inc.). A bundle of eight single-mode detection fibers coupled diffuse light emerging from the head onto two detection arrays of four single-photon-counting avalanche photodiodes (SPCM-AQ4C, Excelitas Technologies, Corp.). Calculation of the intensity autocorrelation curve for each detector was accomplished using a commercial eight-channel correlator board (FLEX03OEM-8CH,

Correlator.com) with a fixed integration time of 3 s per measurement. The tissue absorption and scattering coefficients, measured concurrently over the same tissue volume by FD-DOS, were used as inputs for the calculation of BFI from the intensity autocorrelation curve, averaged across all co-located detection fibers; the calculation was based on the semi-infinite homogeneous medium approximation of the diffusion correlation equation.<sup>54</sup> Individual measurements were rejected when the average detected photon count rate (light intensity) was  $<5\text{ kHz}$ , when the intensity autocorrelation curve failed to decay below 1.01, or when the fit of the intensity autocorrelation curve had greater than 10% error from the sampled curve.

For validation of DCS against invasive laser Doppler, relative CBF from DCS ( $rCBF_{DCS}$ , %) was computed from BFI normalized to the mean baseline BFI value.

### Calculation of cerebral metabolic rate of oxygen

Cerebral metabolic rate of oxygen ( $CMRO_2$ ) was calculated using the Fick principle<sup>55</sup>

$$CMRO_2 = CaO_2 - OEF \cdot CBF \quad (2)$$

where  $CaO_2$  is the arterial blood concentration of oxygen and  $OEF$  is the cerebral  $OEF$ .

**Invasive calculation of  $CMRO_2$ .** Systemic arterial hematocrit (Hct, %), arterial oxygen saturation ( $SaO_2$ , %) and jugular venous oxygen saturation ( $SjvO_2$ , %) were determined at each blood gas sampling time-point and assumed to estimate cerebral arteriole and venule oxygen content, respectively.<sup>56</sup> Using the piglet-specific mean corpuscular hemoglobin concentration (MCHC) of 32.2 g/mL<sup>57</sup> and a mammalian hemoglobin oxygen binding capacity of 1.36 mL  $O_2$ /g Hgb,<sup>58</sup>  $OEF$  and  $CaO_2$  were computed as

$$OEF = \frac{SaO_2 - SjvO_2}{SaO_2} \quad (3)$$

$$CaO_2 = \frac{1.36\text{mLO}_2}{1\text{gHgb}} \cdot \text{Hct}(\%) \cdot \text{MCHC} \left( \frac{\text{gHgb}}{\text{mLblood}} \right) \cdot SaO_2(\%) \quad (4)$$

Continuous laser Doppler measurements of relative CBF ( $rCBF_{LD}$ , %) were calculated with respect to the mean baseline value such that the baseline blood gas draws at the start of cooling corresponded to an  $rCBF_{LD}$  of 100%. For each subsequent blood gas sample, the mean  $rCBF_{LD}$  value in the 30 s preceding the time of blood gas draw was used.  $CaO_2$  and  $OEF$  were also

normalized to baseline and combined into an invasive measure of relative  $CMRO_2$  (invasive  $rCMRO_2$ , %)

$$Invasive\ rCMRO_2 = \frac{CaO_2}{CaO_{2,baseline}} \frac{OEF}{OEF_{baseline}} \frac{rCBF\ LD}{rCBF\ LD_{baseline}} \quad (5) \leftarrow$$

**Non-invasive FD-DOS/DCS calculation of  $CMRO_2$ .** Non-invasive  $CMRO_2$  calculation utilized the baseline arterial blood gas oxygen concentration ( $CaO_{2,baseline}$ , %); this was assumed to remain constant.  $OEF$  was derived from FD-DOS-measured cerebral tissue oxygen saturation ( $StO_2$ , %), baseline arterial oxygen saturation ( $SaO_{2,baseline}$ , %), and an assumed cerebral arteriovenous mixing fraction ( $\gamma$ ) of 0.75<sup>59-61</sup>

$$OEF = \frac{SaO_{2,baseline} - StO_2}{SaO_{2,baseline}} \quad (6) \leftarrow$$

The DCS-measured BFI was used as a surrogate for CBF. Baseline  $CaO_2$ ,  $OEF$ , and BFI, were combined into an absolute index of non-invasive  $CMRO_2$  ( $CMRO_{2,i}$ ), calculated continuously as<sup>18,26,62</sup>

$$CMRO_{2,i} = CaO_{2,baseline} \ OEF \ BFI \quad (7) \leftarrow$$

For comparison with invasive quantification, a relative non-invasive  $CMRO_2$  (non-invasive  $rCMRO_2$ , %) was also calculated for each blood gas sample. Corresponding non-invasive  $OEF$  and BFI values were calculated as the mean value measured in the 30 s prior to blood gas draw. These values were then normalized to their respective baseline blood gas values and, assuming constant  $CaO_2$  and  $\gamma$ , were combined to calculate non-invasive  $rCMRO_2$

$$Noninvasive\ rCMRO_2 = \frac{OEF}{OEF_{baseline}} \frac{BFI}{BFI_{baseline}} \quad (8) \leftarrow$$

### Modeling $CMRO_2$ temperature-dependence

The van't Hoff equation has been widely applied in human and animal studies to describe the relationship between temperature and cerebral metabolism.<sup>7,63</sup> Here, we also employ the van't Hoff equation, either reformulated as the empirical Arrhenius equation<sup>64,65</sup> (equation (9)) or as the  $Q_{10}$  temperature coefficient (equation (11)), to quantify the temperature-dependence of cerebral oxygen metabolism.

**Arrhenius equation approach.** In the Arrhenius relationship (equation (9)), a rate of reaction ( $k$ ) depends on

temperature ( $T$ ), the universal gas constant ( $R$ ), an activation free energy barrier ( $E_a$ ), and a pre-exponential factor ( $A$ ) which is related to the reaction attempt frequency

$$k = Ae^{-\frac{E_a}{RT}} \quad (9) \leftarrow$$

Here we assume this rate of reaction ( $k$ ) to be the metabolic rate,  $CMRO_2$ . Rearrangement and substitution yield a linear expression ( $y = ax + b$ ) that models the relationship between  $CMRO_2$  and temperature

$$\ln(CMRO_2) = \frac{E_a}{R} \left( \frac{1}{T} \right) + \ln(A) \quad (10) \leftarrow$$

Model parameters,  $a = \frac{E_a}{R}$ ,  $b = \ln(A)$ , are obtained from data using linear regression.

**Assessment of model accuracy.** Arrhenius-type approaches, such as the version we utilize, represent an oversimplification of cerebral metabolism, which depends on many chemical reactions and other factors.<sup>7</sup> The model selection we have made might be valid, for example, if a single rate-limiting reaction exists for the metabolic process, or if multiple important reactions had roughly the same free energy barrier height. Dense temperature sampling in vitro has shown good agreement<sup>66</sup>; however, multiple reports of in vivo characterization using sparse sampling methods have found non-Arrhenius or multiphasic behavior, depending on temperature range.<sup>10,67,68</sup> Thus, using continuous quantification of non-invasive  $CMRO_{2,i}$  and temperature, we evaluated model robustness in vivo by goodness-of-fit of the linear regression (equation (10)).

**Temperature coefficient,  $Q_{10}$ .** Most commonly, the temperature-dependence of metabolism has been assessed using the *temperature coefficient*,  $Q_{10}$ . This metric is a reduction of the van't Hoff equation for use under physiologic conditions (see Supplementary Materials, Section S.2).  $Q_{10}$  is defined as the relative change in cerebral metabolic rate per 10°C change in temperature. It can be calculated using an initial and subsequent measurement of temperature and  $CMRO_2$

$$Q_{10} = \left( \frac{CMRO_{2,1}}{CMRO_{2,2}} \right)^{\frac{10}{T_1 - T_2}} \quad (11) \leftarrow$$

The  $Q_{10}$  for both invasive and non-invasive  $rCMRO_2$  measurements was quantified with respect to nasopharyngeal and ICTs.

### Statistical analysis

All statistical analyses were carried out using MATLAB 2014a. Summary statistics were reported as mean and standard deviation, unless otherwise noted.

Continuous time-series data were synchronized using 15 s epoch averages.

The sufficiency of NPT guidance was assessed via the relationship between *non-invasive* NPT and *invasive* ICT, and especially via the functional relationship between non-invasive  $CMRO_{2,i}$  and each temperature source during cooling and rewarming (i.e. using the linear form of the Arrhenius equation; equation (10)). These relationships were individually examined using linear mixed-effects models that incorporated subject-specific random intercept and slope effects to allow for variation in the intercept and slope among individuals. To quantify the potential hysteresis between cooling and rewarming periods, each model included period-specific (e.g. cooling, rewarming) fixed slope (**a**, **a**) and intercept (**b**, **b**) effects reported as mean and standard error. The modeled relationship during *cooling* is expressed as

$$y = ax + b \quad (12) \leftarrow$$

and the modeled relationship during *rewarming* expressed as

$$y = (a + \leftarrow a)x + (b + \leftarrow b) \quad (13) \leftarrow$$

Parameters  $\Delta a$  and  $\Delta b$  should be interpreted as the incremental effects of rewarming on the slope (**a**) and intercept (**b**), respectively, of cooling. The goodness-of-fit of these models was evaluated using the coefficient of determination ( $R^2$ ) of a separate generalized linear regression model with slope and intercept interaction terms for each subject and period.

Validation of non-invasive against invasive  $CMRO_2$  measures at discontinuous blood gas sampling time-points was conducted by paired *t*-test, assuming equal variances and evaluated at a pooled significance level of  $\alpha = 0.05$  with Bonferroni correction for multiple comparisons. Consequently, the five individual time-point *t*-tests were evaluated at an adjusted significance level of  $\alpha = 0.01$ . Given a type II error rate of  $\beta = 0.2$  and an assumed within-subject correlation of 0.875, the analysis was powered to detect a 10% difference in paired observations. Secondly, to assess the *continuous* relationship between *invasive*  $rCBF$  LD versus *non-invasive*  $rCBF$  DCS and *invasive*  $rCMRO_2$  versus *non-invasive*  $rCMRO_2$ , linear mixed-effects models with random slope effects were used to quantify the slope relating the change from baseline ( $rCBF$ , %;  $rCMRO_2$ , %; respectively) between modalities; slope is reported as mean and standard error. To balance continuous  $rCBF$  data across the full range of temperatures from normothermia to DH, the synchronized time-series data were bin-averaged by corresponding temperature in 1°C intervals from 18°C to 37°C. Linearity was

evaluated by the goodness-of-fit, as described above. Finally, agreement between non-invasive measures versus invasive measures of  $rCBF$  and  $rCMRO_2$  was evaluated by the bias and precision from repeated-measures Bland–Altman analysis.<sup>69,70</sup>

Calculated  $CMRO_2 Q_{10}$  coefficients for both nasopharyngeal and ICT-dependence were compared between modalities and to values reported in the literature. Due to their non-normal sample distributions, these results were reported as median and interquartile range (IQR), and intra-subject  $Q_{10}$  comparisons were made using the Wilcoxon signed-rank test.

## Results

Neonatal swine ( $n = 8$ ), with a mean (SD) weight of 4.1 (0.5) kg, were cooled to DH in 25.7 (5.3) min, maintained at DH for 42.6 (1.1) min, and subsequently rewarmed to normothermia in 27.2 (7.0) min.

Summary statistics of experimental parameters are listed in Table 1.

### Temperature-dependence of cerebral oxygen metabolism: Comparison of nasopharyngeal and ICT

Here we examine the impact of NPT guidance on cerebral metabolic parameters. An example of non-invasive optical time-series data is available in Supplementary Materials, Section S.3. The mean and standard deviation of the non-invasive optical measurements of  $OEf$ ,  $rCBF$  DCS, and  $rCMRO_2$  with respect to NPT during cooling and rewarming periods is plotted in Figure 3. Cooling to DH caused a decrease in all parameters. During rewarming,  $OEf$  values are in agreement with cooling, but a hysteresis in  $rCBF$  and  $rCMRO_2$  is apparent.

Characterization of the relationship of NPT and ICT provided additional insights regarding the hysteresis (Figure 4, left). A significant slope effect ( $a = 0.63$  [0.06],  $p < 0.001$ ) confirmed an association between the two temperature monitors with the effect size  $< 1$  indicating a lag of ICT behind NPT (Figure 4, left). Significant rewarming slope ( $\Delta a = -0.08$  [0.01],  $p < 0.001$ ) and intercept ( $\Delta b = -5.0$  [0.3],  $p < 0.001$ ) effects demonstrated a hysteresis between the two temperature monitors with an increased lag and offset in ICT. The mismatch in ICT between the end of cooling and the beginning of rewarming indicated that, despite NPT indicating attainment of DH, the brain had not reached thermal equilibrium.

The NPT-dependence of non-invasive  $CMRO_{2,i}$  exhibited a significant slope effect ( $a = -3.7$  [0.4]  $10^3$ ,  $p < 0.001$ ) which verified an association between metabolism and temperature (Figure 4, center). Confirming the observed hysteresis, rewarming

**Table 1.** Summary statistics.

	Start of cooling	End of cooling	Start of rewarming	End of rewarming
<b>Arterial blood gas<sup>a</sup></b>				
pH	7.4 (0.1)	7.1 (0.1)	7.1 (0.1)	7.4 (0.1)
pCO <sub>2</sub> (mmHg)	45.8 (17.2)	86.5 (16.9)	83.3 (20.5)	39.8 (8.4)
pO <sub>2</sub> (mmHg)	278.6 (92.7)	327.3 (58.5)	286.6 (34.8)	181.7 (80.5)
Glu (umol/L)	163.9 (56.1)	156.1 (45.7)	162.9 (37.7)	142.1 (36.7)
Lac (mmol/L)	3.5 (1.2)	3.8 (1.2)	4.1 (1.4)	6.0 (4.9)
Hct (%)	29.9 (2.8)	29.3 (6.4)	33.2 (7.5)	35.6 (7.0)
HCO <sub>3</sub> (mmol/L)	29.5 (3.1)	29.6 (3.2)	27.2 (5.0)	24.8 (2.9)
SaO <sub>2</sub> (%)	99.2 (2.5)	100.0 (0.0)	99.9 (0.2)	98.8 (2.3)
<b>Invasive neuromonitoring</b>				
ICT (°C)	34.5 (2.4)	22.6 (2.1)	18.8 (1.1)	30.2 (3.1)
PbtO <sub>2</sub> (mmHg)	8.0 (2.7)	8.6 (4.9)	11.1 (8.7)	6.2 (4.9)
SjvO <sub>2</sub> (%) <sup>a</sup>	76.6 (13.2)	95.3 (5.3)	97.3 (2.2)	84.2 (7.3)
OEF	0.23 (0.13)	0.047 (0.053)	0.026 (0.022)	0.15 (0.06)
rCBF LD (%)	100.0 (-)	45.9 (18.1)	41.9 (21.2)	49.4 (9.9)
rCMRO <sub>2</sub> (%)	100.0 (-)	9.3 (9.9)	3.4 (3.2)	32.3 (7.9)
<b>Non-invasive neuromonitoring</b>				
NPT (°C)	37.3 (0.5)	17.8 (0.3)	18.2 (0.5)	37.3 (0.5)
$\mu_a$ (1/cm)				
$\lambda = 690$ nm	0.17 (0.02)	0.14 (0.02)	0.15 (0.02)	0.19 (0.03)
$\lambda = 725$ nm	0.14 (0.02)	0.13 (0.02)	0.14 (0.01)	0.16 (0.02)
$\lambda = 785$ nm	0.14 (0.02)	0.15 (0.03)	0.15 (0.03)	0.16 (0.03)
$\lambda = 830$ nm	0.15 (0.02)	0.16 (0.03)	0.17 (0.03)	0.17 (0.02)
$\mu_s'$ (1/cm)				
$\lambda = 690$ nm	12.2 (1.7)	11.6 (1.6)	11.7 (1.3)	12.4 (1.6)
$\lambda = 725$ nm	10.2 (1.5)	10.0 (1.4)	10.1 (1.2)	10.6 (1.6)
$\lambda = 785$ nm	9.9 (1.5)	10.0 (1.5)	10.0 (1.4)	10.3 (1.7)
$\lambda = 830$ nm	9.4 (2.0)	10.1 (2.1)	9.9 (1.8)	9.9 (1.7)
THC ( $\mu\text{mol/L}$ )	75.3 (9.3)	81.0 (14.0)	85.1 (14.9)	86.1 (12.6)
StO <sub>2</sub> (%)	57.2 (5.3)	68.6 (8.7)	69.9 (11.4)	58.6 (6.7)
OEF	0.56 (0.07)	0.41 (0.10)	0.39 (0.14)	0.54 (0.08)
BFI ( $10^{-8}$ cm <sup>2</sup> /s)	1.2 (1.2)	0.57 (0.55)	0.49 (0.51)	0.69 (0.73)
rCBF DCS (%)	100.0 (-)	50.1 (17.5)	45.9 (28.9)	64.5 (31.6)
rCMRO <sub>2</sub> (%)	100.0 (-)	35.8 (8.7)	27.8 (11.4)	63.2 (35.5)

<sup>a</sup>Values are corrected to 37°C. Glu: Glucose; Lac: Lactate; Hct: Hematocrit; SjvO<sub>2</sub>: internal jugular venous oxygen saturation; rCBF LD: relative cerebral blood flow measured using laser Doppler; ICT: intracranial temperature; PbtO<sub>2</sub>: partial pressure of oxygen in brain tissue; StO<sub>2</sub>: cerebral tissue oxygen saturation from FD-DOS; BFI: blood flow index measured using DCS; rCBF DCS: relative cerebral blood flow measured using DCS; NPT: nasopharyngeal temperature; THC: total hemoglobin concentration measured using FD-DOS.

had a significant and dampening effect on slope ( $\mathbf{a} = +1.4 [0.4] 10^3$ ,  $p = 0.001$ ), which suggests metabolism had diminished sensitivity to NPT. Linear regression resulted in a strong coefficient of determination ( $R^2 = 0.87$ ) and affirms use of Arrhenius-type models for examining cerebral metabolic temperature-dependence at physiologic temperatures. The ICT-dependence of non-invasive  $CMRO_{2,i}$  also demonstrated a strong coefficient of determination with linear regression ( $R^2 = 0.90$ ) and had a significant slope effect

( $\mathbf{a} = -5.2 [1.0] 10^3$ ,  $p < 0.001$ ; Figure 4, right). Surprisingly, rewarming did not have a significant effect on slope ( $\mathbf{a} = +0.3 [0.6] 10^3$ ,  $p = 0.647$ ) or intercept ( $\mathbf{b} = -1.1 [2.1]$ ,  $p = 0.585$ ).

These results highlight critical insufficiencies of NPT guidance to accurately reflect ICT or metabolic status during DH CPB. Furthermore, they suggest that the presence of cerebral metabolic hysteresis with respect to temperature may be an artifact resulting from use of NPT to approximate ICT.

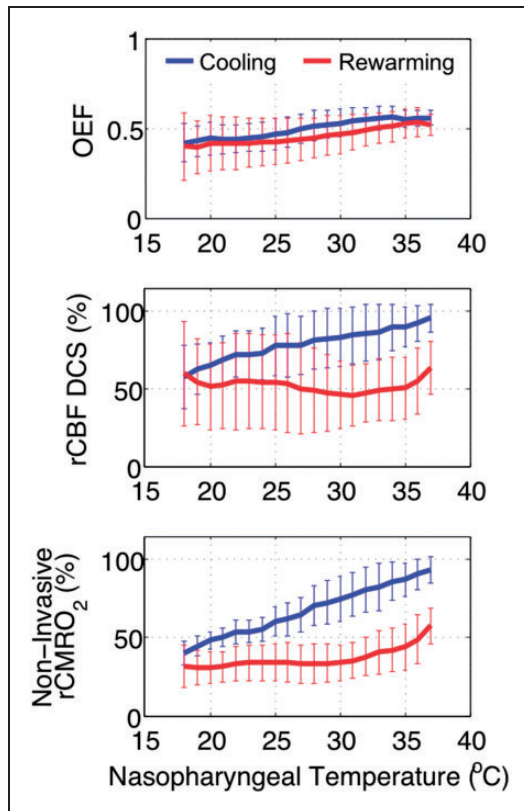


**Figure 3.** Temperature-dependence of non-invasive optical measures of cerebral oxygen extraction fraction, flow, and metabolism during cooling (blue) from normothermia to deep hypothermia, and during rewarming (red) from deep hypothermia back to normothermia. Mean values across subjects ( $n=8$ ) are plotted along with standard deviation. Abbreviations: *OEF*: oxygen extraction fraction; *rCBF DCS*: DCS measure of relative cerebral blood flow; *rCMRO<sub>2</sub>*: relative cerebral metabolic rate of oxygen.

### Validation of non-invasive quantification of cerebral oxygen metabolism

The results of models examining discontinuous and continuous repeated measures of *CMRO<sub>2</sub>* parameters to assess differences between invasive and non-invasive modalities are reported. Blood gas analysis was hampered by a machine malfunction in a single animal, resulting in the inclusion of seven of eight animals.

**Arterial concentration of oxygen (*CaO<sub>2</sub>*).** *CaO<sub>2</sub>* quantified discontinuously from invasive blood gas samples, were used to examine the non-invasive assumption that *CaO<sub>2</sub>* remained constant through DH and recovery to normothermia. Importantly, no significant differences from baseline were observed in relative *CaO<sub>2</sub>* (*rCaO<sub>2</sub>*; Figure 5, top left). From these results, we conclude that the assumption of constant *CaO<sub>2</sub>* for non-invasive quantification during DH was reasonable.

***OEF*.** Significant differences between non-invasive versus discontinuous invasive measures of relative *OEF* (*rOEF*; Figure 5, top right) were found at the end of cooling (difference = +53.9% (24.3),  $p=0.001$ ), start of rewarming (difference = +62.4% (22.6),  $p<0.001$ ), midpoint of rewarming (difference = +50.8% (20.4),  $p=0.002$ ), and end of rewarming (difference = +34.2% (17.2),  $p=0.005$ ). Non-invasive sampling demonstrated consistently greater *rOEF* across all time-points.

The non-invasive calculation of *OEF* is derived from baseline blood gas *SaO<sub>2</sub>* and from continuous non-invasive measurement of cerebral tissue oxygen saturation (*StO<sub>2</sub>*; equation (6)). Given the limited range in *SaO<sub>2</sub>* (98.0–100.0%) during cooling and rewarming, significant differences in non-invasive and invasive *OEF* must be attributed to a disagreement between non-invasive *StO<sub>2</sub>* and invasive sampling of jugular venous oxygen saturation (*SjvO<sub>2</sub>*). Additional analysis of the relationship of *StO<sub>2</sub>* and *SjvO<sub>2</sub>* is included in Supplementary Materials, Section S.4.

***CBF*.** Non-invasive, continuous *rCBF DCS* measurement demonstrated good agreement with invasive, continuous *rCBF LD*. Significant differences were not found at all discontinuous blood gas sampling time-points (Figure 5, bottom left). Examination of the *continuous* relationship between modalities demonstrated that the change from baseline (*rCBF*, %) of non-invasive DCS significantly predicted (Figure 6, left) invasive laser Doppler with a slope effect of 1.26 [0.15] ( $p<0.001$ ). Linear regression with subject-specific slope interactions resulted in a good coefficient of determination ( $R^2=0.73$ ), suggesting a strong linear relationship between modalities. Using Bland–Altman analysis, the comparison of mean *rCBF* (%) between modalities was found to have a bias of –10.0% and precision of 13.1% (Supplementary Materials, Section S.5). These findings support the use of DCS for non-invasive measurement of *rCBF* during DH CPB.

***CMRO<sub>2</sub>*.** Non-invasive versus invasive relative *CMRO<sub>2</sub>* measured discontinuously exhibited significant differences at the end of cooling (difference = +26.9% (9.7),  $p<0.001$ ), start of rewarming (difference = +25.1% (11.7),  $p=0.001$ ), and midpoint of rewarming (difference = +18.3% (8.1),  $p=0.003$ ; Figure 5, bottom right). Due to the dependence of *CMRO<sub>2</sub>* on *OEF*, significant differences in *rOEF* directly contributed to differences in *rCMRO<sub>2</sub>*, whereby non-invasive sampling reflected higher levels of metabolism versus invasive sampling.

Examination of the continuous relationship between modalities by linear mixed-effects model analysis

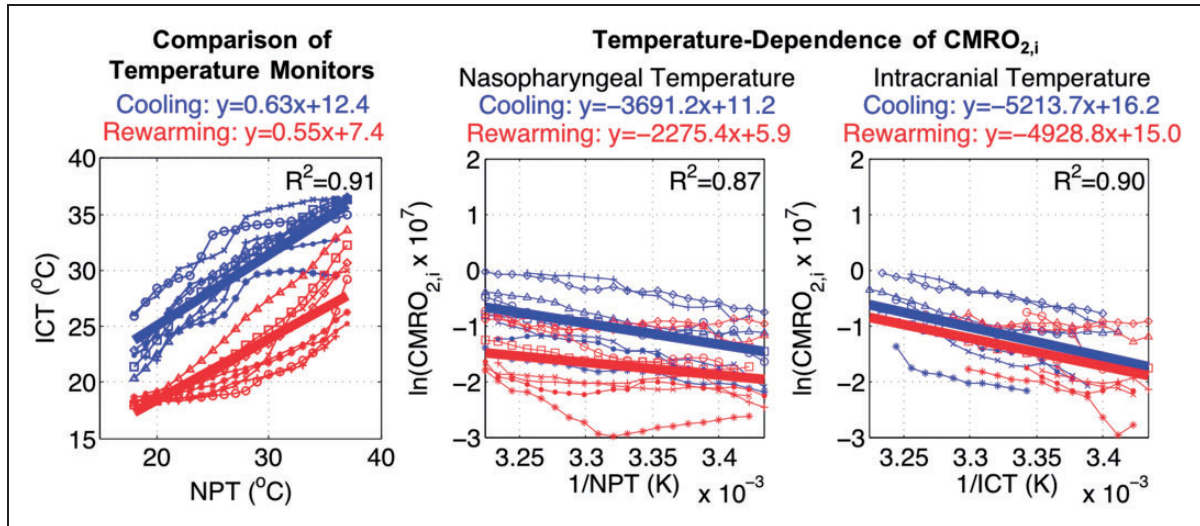


**Figure 4.** (Left) Intracranial temperature hysteresis: significant hysteresis of intracranial temperature (ICT) with respect to nasopharyngeal temperature (NPT) during rewarming (red) versus cooling (blue); rewarming slope  $p < 0.001$ , intercept  $p < 0.001$ . Non-invasive  $CMRO_{2,i}$  Temperature-dependence: (Center)  $CMRO_{2,i}$ , with respect to  $(NPT)^{-1}$ , also demonstrates significant hysteresis in rewarming slope ( $p = 0.001$ ) and intercept ( $p < 0.001$ ). (Right)  $CMRO_{2,i}$ , with respect to  $(ICT)^{-1}$ , has improved concordance between rewarming versus cooling; rewarming slope  $p = 0.647$ , intercept  $p = 0.585$ . Thick lines represent fitted linear mixed-effects models; unique symbols connected by thin lines represent individual subject data ( $n = 8$ ).

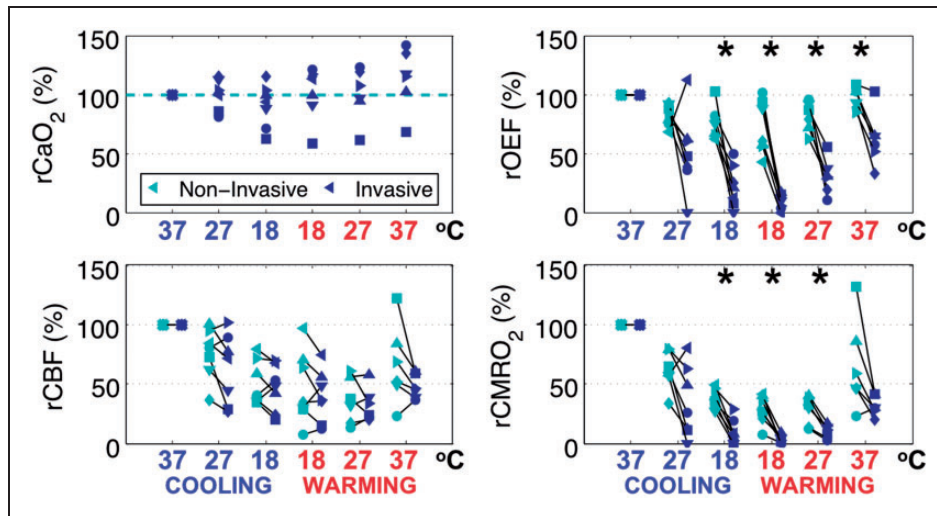


**Figure 5.** Comparison of invasive versus non-invasive tissue sampling at each blood gas time-point demonstrate validity of optical assumptions of arterial concentration of oxygen ( $CaO_2$ ), agreement of relative cerebral blood flow ( $rCBF$ ) measurements, but a discrepancy in relative oxygen extraction fraction ( $rOEF$ ) and relative metabolic rate of oxygen ( $rCMRO_2$ ). Paired data at each time-point are displayed with a unique symbol for each subject ( $n = 7$ ) colored by modality (i.e. non-invasive, green; invasive, blue), and the x-axis labeled by respective nasopharyngeal temperature with stage designated by color (i.e. cooling, blue; rewarming, red). Asterisks (\*) denote significant differences ( $p < 0.01$ ) in paired  $t$ -tests between invasive and non-invasive sampling.

demonstrated that non-invasive  $rCMRO_2$  (%) significantly predicted (Figure 6, right) invasive  $rCMRO_2$  (%) with a slope effect of 1.31 [0.07] ( $p < 0.001$ ); however, linear regression resulted in only a fair coefficient of determination ( $R^2 = 0.53$ ) suggesting underlying non-linearity. Using Bland-Altman analysis, agreement

of  $rCMRO_2$  between modalities was found to have a bias of  $-25.8\%$  and precision of  $12.5\%$  (Supplementary Materials, Section S.4). Despite modest quantitative agreement, these findings show a highly significant association between non-invasive and invasive  $rCMRO_2$  measurements; this association, in

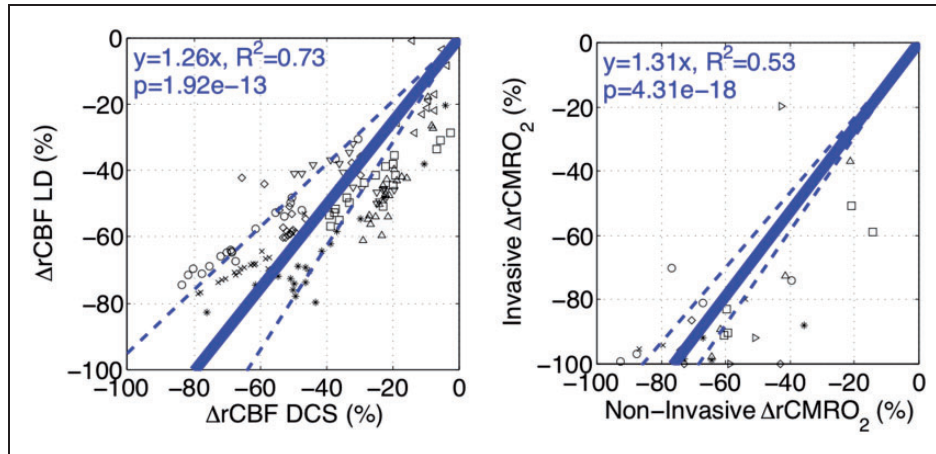


**Figure 6.** Validation of non-invasive diffuse correlation spectroscopy (DCS, left) and  $CMRO_2$  (right) – data from individual subjects are indicated by a unique symbol. Measurements of change in relative cerebral blood flow using laser Doppler ( $rCBF_{LD}$ , %) and DCS ( $rCBF_{DCS}$ , %) are compared using a linear mixed-effects model ( $n = 8$ ; left). DCS measurements demonstrate a good linear correlation (fixed slope effect  $p < 0.001$ ;  $R^2 = 0.73$ ) against laser Doppler measurements. Similarly, invasive and non-invasive measurements of  $rCMRO_2$  (%) are compared using a linear mixed-effects model ( $n = 7$ ; right). Non-invasive  $rCMRO_2$  quantification demonstrates a significant association but limited linearity (fixed slope effect  $p < 0.001$ ;  $R^2 = 0.53$ ) against invasive sampling. Fitted linear relationships (solid line) with 95% confidence intervals (dotted line) are plotted in blue.

turn, supports use of non-invasive measurements as an indicator of cerebral status.

**$CMRO_2$  temperature coefficient ( $Q_{10}$ ).** Computed  $CMRO_2$  temperature coefficient  $Q_{10}$  derived from invasive sampling differed significantly from that of non-invasive sampling, whether assessed with respect to NPT (non-invasive versus invasive median [IQR]: 2.0 [1.6, 2.3] versus 4.9 [3.6, 6.3],  $p = 0.016$ ) or ICT (non-invasive versus invasive median [IQR]: 2.5 [2.0, 3.5] versus 9.0 [6.9, 11.0],  $p = 0.016$ ). This finding further affirms our discrepant findings at individual blood gas sampling time-points. As may be expected from the presence of significant temperature hysteresis,  $Q_{10}$  based on ICT was significantly different from  $Q_{10}$  based on NPT, i.e. whether measured non-invasively (NPT versus ICT median [IQR]: 2.0 [1.6, 2.3] versus 2.5 [2.0, 3.5],  $p = 0.016$ ) or invasively (NPT versus ICT median [IQR]: 4.9 [3.6, 6.3] versus 9.0 [6.9, 11.0],  $p = 0.016$ ). Regardless of metabolic sampling method, sensitivity to NPT was lower than to ICT.

## Discussion

Continuous, non-invasive optical metabolic neuromonitoring using FD-DOS combined with DCS permits understanding of the physiologic alterations of cerebral metabolism that occur during therapeutic hypothermia. This approach has the potential to address critical shortfalls in conventional temperature guidance of hypothermia, as well as to enable individualized

neuroprotective strategies. The present study takes important steps towards this goal.

### Temperature-dependence of cerebral oxygen metabolism: Comparison of nasopharyngeal and ICT

NPT is an established source of guidance for DH CPB management<sup>1</sup> and has been found, among other non-invasive sites of core temperature measurement, to best approximate cerebral temperature.<sup>41</sup> However, our data add to mounting evidence that NPT does not adequately reflect ICT, nor the metabolic state of the brain.<sup>71,72</sup> This finding is evident from the metabolic hysteresis with respect to NPT between cooling and rewarming periods, and in the significantly different temperature coefficients exhibited by nasopharyngeal versus ICT. The finding that ICT has more concordant metabolic temperature-dependence between cooling and rewarming periods is supported by prior in vitro observations of the reversibility of hypothermic metabolic inhibition.<sup>66</sup> The continued decline of ICT following cooling indicates the clinical cooling interval used was insufficient for thermal equilibrium and underscores the importance of directly measuring the metabolic state of the brain in lieu of using NPT as a surrogate.

By coupling continuous FD-DOS/DCS measurements of cerebral oxygen metabolism with continuous temperature measurements during DH, we were additionally able to examine the validity of temperature-dependent models for the metabolic rate based on the

Arrhenius equation. These models were consistent with our data, whether using NPT ( $R^2=0.87$ ) or ICT ( $R^2=0.90$ ). Our results support the continued use of  $Q_{10}$  to characterize the temperature-dependence of cerebral oxygen metabolism.

### Validation of non-invasive quantification of cerebral oxygen metabolism

Non-invasive  $rCMRO_2$  significantly predicted invasive  $rCMRO_2$  ( $p < 0.001$ ). However, we found significant discrepancies in measured values with a bias of  $-25.8\%$  and precision of  $12.5\%$ . This mismatch is discussed, and rationalized, with respect to each component of the  $CMRO_2$  calculation below.

**Arterial concentration of oxygen.** A critical assumption of non-invasive  $CMRO_2$  quantification is that  $CaO_2$  remains constant from baseline. While increases in  $CaO_2$  are expected during hypothermia,<sup>73</sup> avoidance of hyperoxia during CPB has been established.<sup>74</sup> Fortuitously, oxygen administration is intentionally adjusted during hypothermia to maintain constant arterial blood oxygen tension. In-line with these recommendations, we found that only the last sampling time-point after recovery to normothermia demonstrated a significant difference from baseline. Thus, the assumption of constant  $CaO_2$  for non-invasive quantification during deep hypothermic CPB seems reasonable and is concordant with invasive sampling.

**OEF.** Absolute OEF was found to differ significantly between invasive and non-invasive sampling methods at all time-points. We determined that this effect resulted from a disagreement between optically measured cerebral tissue oxygen saturation ( $StO_2$ ), and the compartment model computation of  $StO_2$  via  $StO_2 = (1-\gamma)SaO_2 + \gamma SjvO_2$ , wherein an arteriovenous mixing fraction of  $\gamma = 0.75$  was assumed.<sup>59,61</sup> In fact,  $StO_2$  was consistently lower than  $SjvO_2$ , thus violating a necessarily positive  $\gamma$ . This phenomenon has been reported in the context of CW NIRS instruments and FD-DOS measurements in animals models<sup>47,75</sup> and human subjects,<sup>16,60</sup> and remains to be further explored in future studies. Our findings support the reproducibility of this phenomenon and sheds further light on the issue.

The use of jugular venous sampling in this study was based on its wide utilization in pediatric cardiac surgery for this purpose<sup>8,76</sup> and for comparison with non-invasive cerebral oximetry.<sup>60,77-79</sup> Prior reports of jugular venous sampling in swine models of CPB agree with our observations. In Sasaki et al.<sup>75</sup>  $SjvO_2$  were calculated from reported OEF as  $74.5 \pm 7.1\%$  at normothermia and  $89.5 \pm 4.2\%$  at  $18^\circ\text{C}$  in comparably aged

neonatal piglets.<sup>75</sup> In slightly older (three to four weeks) and larger piglets ( $9.4 \pm 0.8\text{kg}$ ), Walther et al.<sup>36</sup> reported  $SjvO_2$  of  $86-88\%$  at normothermia,  $91\%$  at a body temperature of  $25^\circ\text{C}$ , and  $93\%$  at a body temperature of  $18^\circ\text{C}$ .<sup>36</sup> While these values are in the range of our  $SjvO_2$  measurements at normothermia ( $76.6 \pm 13.2\%$ ) and at DH ( $95.3 \pm 5.3\%$ ), further comparison with sagittal sinus sampling suggests these measurements may have been affected by reported limitations of jugular venous sampling to access cerebral venous saturation.<sup>80</sup>

Animal studies wherein sagittal sinus oxygen saturation ( $SssO_2$ ) was directly sampled during hypothermic CPB show consistently lower values than reported  $SjvO_2$ . Two observations in moderately larger piglets ( $5-13\text{kg}$ ) reported an  $SssO_2$  of  $75 \pm 10\%$  at normothermia and  $85 \pm 5\%$  at DH ( $18-20^\circ\text{C}$ ).<sup>12,35</sup> While normothermic values are comparable to our observations, hypothermic saturations are markedly lower. These comparisons indicate that internal jugular venous sampling overestimates sagittal sinus saturations, resulting in an underestimation of true cerebral OEF in pediatric swine models. We believe this to be the primary source of error in our invasively quantified OEF and, subsequently,  $CMRO_2$ .

Probable physiologic mechanisms that could elevate  $SjvO_2$  with respect to  $SssO_2$  include systemic venous contamination of jugular venous sampling due, in part, to the logistical difficulty of advancing a catheter into small neonatal vessels. Contributions from the external jugular vein or superior vena cava would reflect higher saturations due to lower somatic oxygen utilization rates compared to the brain. This hypothesis is corroborated by central venous saturations of  $75\%$  at normothermia and  $98 \pm 2\%$  at  $18^\circ\text{C}$  in Cavus et al.,<sup>35</sup> our  $SjvO_2$  agrees at baseline and is only  $3\%$  lower at DH. Future studies conducted in neonatal swine should be wary of systemic contributions with this sampling method that may inaccurately diminish cerebral OEF.

**CBF.** Significant agreement was observed between invasive laser Doppler (LD) and non-invasive DCS measurement of CBF throughout DH. Our invasive data, in particular, advance recent cross-validation of DCS with TCD.<sup>29</sup> In principle, quantitative variation between LD and DCS can be attributed to regional variability in metabolic and cerebrovascular response to hypothermia, which has been previously reported,<sup>81-83</sup> and can also result from extracerebral contributions to the optical signal.<sup>84-86</sup> Measuring tissue thickness post-mortem, we found  $0.5\text{cm}$  of superficial tissue (e.g. skull, scalp) above the brain. The potential contribution from this tissue should be explored in future studies using advanced multi-layered optical extraction.

$CMRO_2$ . Taken in total, non-invasive optical measurement of  $CMRO_2$  demonstrated lower temperature-sensitivity and higher residual metabolic rates at DH than invasively sampled  $CMRO_2$ . As discussed above, we believe this to be a direct result of systemic contributions to invasive jugular venous sampling. For further validation, calculated  $Q_{10}$  temperature coefficients were compared to those reported in the literature.

In studies utilizing non-invasive temperature methods and jugular venous sampling, Greeley et al.<sup>8</sup> reported an average  $Q_{10}$  of 3.65 in neonates and children, and McCullough et al.<sup>9</sup> reported a  $Q_{10}$  of 2.3 in adults. While these measurements are potentially confounded by pathologic conditions necessitating the use of hypothermic CPB, plausibility is provided for our non-invasive ( $Q_{10}=2.0$ ) versus invasive ( $Q_{10}=4.9$ ) measurements with respect to NPT.

In healthy animal models with invasive ICT and sagittal sinus sampling, Michenfelder and Milde<sup>10</sup> saw a  $Q_{10}$  of 2.23 for mild hypothermia (ICT between 37°C and 27°C) and 4.53 for DH (27 to 14°C) in canines; CBF was measured using a flow-through electromagnetic flow probe placed in the sagittal sinus.<sup>10</sup> Using both radioactive and fluorescent microspheres for CBF determination, Ehrlich et al.<sup>12</sup> observed a  $Q_{10}$  of 2.46 with a 95% CI of 2.1 to 2.9 (38°C to 8°C) in piglets ranging in weight from 7 to 13 kg.<sup>12</sup> These values support the validity of our non-invasive metabolic measurements, which exhibited a  $Q_{10}$  of 2.5 with respect to ICT, versus our invasive measurements ( $Q_{10}=9.0$ ) which incorporated jugular venous sampling. In sum, despite significant differences between our non-invasive and invasive sampling methods, we are confident that our non-invasive metabolic measurements are in agreement with prior studies of cerebral metabolic temperature-response and hold tremendous clinical promise to measure an individual patient's  $CMRO_2$ .

### Limitations of animal model

Several considerations affect the interpretation of our animal model results for application to neonatal cardiac patients. First, we utilized only female animals; in light of reported sexual dimorphisms with respect to brain development<sup>87</sup> and tolerance to neurological injury,<sup>88,89</sup> further study is required to understand potential sex differences in metabolic temperature-dependence. Additionally, piglet resting core temperatures are slightly higher than human neonates (38.5°C vs. 36.5°C).<sup>82,90</sup> The impact of relative hypothermia in the animal model may have resulted in lower metabolic values than an animal at natural baseline. Variation in anesthetic management, rate and duration of temperature derangement, and the use of circulatory arrest among pediatric cardiac surgical practices may also

impact generalizability.<sup>32,91,92</sup> Notably, the oxygen binding affinity of swine hemoglobin has been shown to be significantly lower than that of human hemoglobin.<sup>93</sup> This effect could account for the lower baseline cerebral oxygen tissue saturations measured versus baseline values in human subjects. Furthermore, there is less impact of cooling on oxygen binding affinity.<sup>94</sup> Therefore, greater changes in cerebral metabolism (i.e. larger temperature coefficients) may be observed in humans than those measured here.

### Clinical applications of cerebral metabolic monitoring during therapeutic hypothermia

Clinical imaging modalities that permit access to cerebral metabolism include stand-alone PET, which typically requires the injection or inhalation of radioactive tracers such as <sup>15</sup>O-H<sub>2</sub>O and <sup>18</sup>F-FDG for glucose metabolism<sup>95</sup> or <sup>15</sup>O<sub>2</sub> gas for oxygen metabolism,<sup>96</sup> and stand-alone MRI,<sup>97</sup> which uses a combination of arterial spin labeling or phase-contrast mapping for CBF and calibrated blood-oxygen-level-dependent T2\* signal mapping for oxygenation. More recently, integrated PET/MRI paradigms that decrease the invasive vascular access requirements of stand-alone PET have been demonstrated.<sup>98</sup> These modalities have profoundly impacted clinical care, as well as our understanding of developmental and pathologic alterations in cerebral metabolism; however, extensive patient transport and operating room requirements, the incremental ionizing radiation exposure of PET, and the prolonged durations and limited throughput associated with MRI data acquisition prohibit real-time, intraoperative monitoring, particularly in neonates.

FD-DOS/DCS sacrifices spatial resolution and sensitivity for temporal resolution and portability that, as specifically demonstrated in the present work, permit real-time guidance during procedural hypothermia. Frequently, neonatal surgical protocols utilize DH for neuroprotection during subsequent circulatory arrest. Temperature of initiation and what duration of circulatory arrest is safe remain controversial.<sup>1,6,99</sup> Precise determination of residual cerebral metabolism using diffuse optics could be used to individually guide cooling to adequate levels of cerebral metabolic suppression as well as provide a subject-specific estimate of safe arrest duration based on rate of [HbO<sub>2</sub>] depletion in cerebral tissue. Alternatively, mild hypothermia has also demonstrated therapeutic potential to improve mortality<sup>100,101</sup> and neurological<sup>102</sup> and neurodevelopmental outcomes<sup>103</sup> in infants with hypoxic-ischemic encephalopathy. Non-invasive optical CW NIRS and FD-DOS/DCS have already been used at the bedside in these infants to examine alterations in cerebral autoregulation<sup>104</sup> and metabolism.<sup>105</sup> We anticipate that

our findings will enable and motivate closer examination of the magnitude and rate of hypothermia-induced cerebral metabolic suppression and neurological outcomes in these patients.

## Conclusions

This study identifies critical limitations in conventional NPT guidance during deep hypothermic CPB in neonates, and it provides strong evidence for the validity and utility of non-invasive diffuse optical measurements of cerebral oxygen metabolism to address these limitations. Continuous measurements throughout cooling and rewarming enabled novel high-fidelity determination of metabolic temperature-dependence in vivo and validation of Arrhenius-type models (i.e. the van't Hoff Law and  $Q_{10}$ ). The relationship between non-invasive  $CMRO_2$  and NPT demonstrated a problematic hysteresis between cooling and rewarming periods. The finding that ICT-dependence improved concordance suggests that NPT inadequately reflects cerebral metabolic state and may be a significant source of uncertainty in the clinical guidance of hypothermia for brain protection. The application of non-invasive FD-DOS/DCS for direct quantification of cerebral oxygen metabolism thus offers promise for improved guidance of therapeutic hypothermia and for mitigation of neurological injury in vulnerable pediatric populations.

## Funding

The author(s) disclosed receipt of the following financial support for the research, authorship, and/or publication of this article: This project was supported by the National Institute of Health through grant numbers R01-NS072338, R01-NS060653, P41-EB015893, F31-HD085731, and the June and Steve Wolfson Family Foundation.

## Acknowledgements

The authors would like to thank the veterinary staff at the Children's Hospital of Philadelphia, Drs. Dean Kurth and William Greeley for lighting the way and their consummate support, Rodrigo Forti, Jeff Cochran, Marin Jacobwitz, Mahima Deverajan, and other members of the June and Steve Wolfson Laboratory and the Yodh Biomedical Optics Group for their constructive discussion and comradery, as well as Dr. Erin Buckley, Peter Lee, and Dr. Rickson Mesquita for their technical guidance.

## Declaration of conflicting interests

The author(s) declared the following potential conflicts of interest with respect to the research, authorship, and/or publication of this article: Authors (in parenthesis) disclose partial ownership of active relevant patents applications. Pending: WO2013/090658A1 (AGY), PCT/US2012/069626

(AGY), PCT/US2015/017286 (AGY, DRB), PCT/US2015/017277 (AGY, DRB). Granted: US8082015B2 (AGY). No author currently receives royalties or payments from these patents.

## Authors' contributions

TSK, CDM, WBB, JML, DRB, JG, RWM, JWJ, TJK, AGY, and DJL contributed to the conception and design of the study. TSK, CDM, VM, KM, TWB, ALS, JG, GDB, YL, SJ, RWM, TMR, BCS, KLS, and TJK contributed to acquisition of data. TK, CDM, WBB, VM, KMB, TWB, ALS, JML, DRB, RX, AGY, TJK, and DJL contributed to analysis and/or interpretation of data. TSK, CDM, and RWM drafted the manuscript. WBB, DRB, RX, AGY, TJK, and DJL contributed to revising the manuscript critically for important intellectual content. All authors have approved the final version of the manuscript for publication.

## Supplementary material

Supplementary material for this paper can be found at the journal website: <http://journals.sagepub.com/home/jcb>

## References

1. Kouchoukos N, Blackstone E, Hanley F, et al. Hypothermia, Circulatory Arrest, and Cardiopulmonary Bypass. In: *Kirklin/Barratt-Boyes Cardiac Surgery*. London, United Kingdom: Elsevier Health Sciences, 2013, pp. 67–132.
2. Mahle WT, Clancy RR, Moss EM, et al. Neurodevelopmental outcome and lifestyle assessment in school-aged and adolescent children with hypoplastic left heart syndrome. *Pediatrics* 2000; 105: 1082–1089.
3. Marino BS, Lipkin PH, Newburger JW, et al. Neurodevelopmental outcomes in children with congenital heart disease: evaluation and management: a scientific statement from the American Heart Association. *Circulation* 2012; 126: 1143–1172.
4. Kirkham FJ. Recognition and prevention of neurological complications in pediatric cardiac surgery. *Pediatr Cardiol* 1998; 19: 331–345.
5. Bellinger DC, Wypij D, Du Plessis AJ, et al. Developmental and neurologic effects of alpha-stat versus pH-stat strategies for deep hypothermic cardiopulmonary bypass in infants. *J Thorac Cardiovasc Surg* 2001; 121: 374–383.
6. Wypij D, Newburger JW, Rappaport LA, et al. The effect of duration of deep hypothermic circulatory arrest in infant heart surgery on late neurodevelopment: the Boston Circulatory Arrest Trial. *J Thorac Cardiovasc Surg* 2003; 126: 1397–1403.
7. Erecinska M, Thoresen M and Silver IA. Effects of hypothermia on energy metabolism in mammalian central nervous system. *J Cereb Blood Flow Metab* 2003; 23: 513–530.
8. Greeley WJ, Kern FH, Ungerleider RM, et al. The effect of hypothermic cardiopulmonary bypass and total circulatory arrest on cerebral metabolism in neonates, infants, and children. *J Thorac Cardiovasc Surg* 1991; 101: 783–94.

9. McCullough JN, Zhang N, Reich DL, et al. Cerebral metabolic suppression during hypothermic circulatory arrest in humans. *Ann Thorac Surg* 1999; 67: 1895–1899.
10. Michenfelder JD and Milde JH. The relationship among canine brain temperature, metabolism, and function during hypothermia. *Anesthesiology* 1991; 75: 130–136.
11. Croughwell ND, Frasco P, Blumenthal JA, et al. Warming during cardiopulmonary bypass is associated with jugular bulb desaturation. *Ann Thorac Surg* 1992; 53: 827–832.
12. Ehrlich MP, McCullough JN, Zhang N, et al. Effect of hypothermia on cerebral blood flow and metabolism in the pig. *Ann Thorac Surg* 2002; 73: 191–197.
13. Austin EH, Edmonds HL, Auden SM, et al. Benefit of neurophysiologic monitoring for pediatric cardiac surgery. *J Thorac Cardiovasc Surg* 1997; 114: 707–717.
14. Neshat Vahid S and Panisello JM. The state of affairs of neurologic monitoring by near-infrared spectroscopy in pediatric cardiac critical care. *Curr Opin Pediatr* 2014; 26: 299–303.
15. Lynch JM, Buckley EM, Schwab PJ, et al. Time to surgery and preoperative cerebral hemodynamics predict postoperative white matter injury in neonates with hypoplastic left heart syndrome. *J Thorac Cardiovasc Surg* 2014; 148: 2181–2188.
16. Lynch JM, Buckley EM, Schwab PJ, et al. Noninvasive optical quantification of cerebral venous oxygen saturation in humans. *Acad Radiol* 2014; 21: 162–167.
17. Lin P-Y, Roche-Labarbe N, Dehaes M, et al. Non-invasive optical measurement of cerebral metabolism and hemodynamics in infants. *J Vis Exp* 2013; e4379.
18. Roche-Labarbe N, Carp SA, Surova A, et al. Noninvasive optical measures of CBV, StO<sub>2</sub>, CBF index, and rCMRO<sub>2</sub> in human premature neonates' brains in the first six weeks of life. *Hum Brain Mapp* 2010; 31: 341–352.
19. Roche-Labarbe N, Fenoglio A, Radhakrishnan H, et al. Somatosensory evoked changes in cerebral oxygen consumption measured non-invasively in premature neonates. *Neuroimage* 2014; 85: 279–286.
20. Ferradal SL, Yuki K, Vyas R, et al. Non-invasive assessment of cerebral blood flow and oxygen metabolism in neonates during hypothermic cardiopulmonary bypass: feasibility and clinical implications. *Sci Rep* 2017; 7: 1–9.
21. Lynch JM. *Investigations of Cerebral Hemodynamics in Infants With Critical Congenital Heart Disease Using Diffuse Optics*. Philadelphia, PA: University of Pennsylvania, 2014.
22. Lynch JM, Ko T, Busch DR, et al. Preoperative cerebral hemodynamics from birth to surgery in neonates with critical congenital heart disease. *J Thorac Cardiovasc Surg* 2018; 156: 1657–1664.
23. Durduran T, Zhou C, Buckley EM, et al. Optical measurement of cerebral hemodynamics and oxygen metabolism in neonates with congenital heart defects. *J Biomed Opt* 2010; 15: 037004.
24. Buckley EM. *Cerebral Hemodynamics in High-Risk Neonates Probed by Diffuse Optical Spectroscopies*. Philadelphia, PA: University of Pennsylvania, 2011.
25. Buckley EM, Lynch JM, Goff DA, et al. Early post-operative changes in cerebral oxygen metabolism following neonatal cardiac surgery: effects of surgical duration. *J Thorac Cardiovasc Surg* 2013; 145: 196–205.e1.
26. Jain V, Buckley EM, Licht DJ, et al. Cerebral oxygen metabolism in neonates with congenital heart disease quantified by MRI and optics. *J Cereb Blood Flow Metab* 2014; 34: 380–388.
27. Busch DR, Lynch JM, Winters ME, et al. Cerebral blood flow response to hypercapnia in children with obstructive sleep apnea syndrome. *Sleep* 2016; 39: 209–216.
28. Dehaes M, Cheng HH, Buckley EM, et al. Perioperative cerebral hemodynamics and oxygen metabolism in neonates with single-ventricle physiology. *Biomed Opt Exp* 2015; 6: 4749.
29. Busch DR, Rusin CG, Miller-Hance W, et al. Continuous cerebral hemodynamic measurement during deep hypothermic circulatory arrest. *Biomed Opt Exp* 2016; 7: 3461–3470.
30. Mezrow CK, Midulla PS, Sadeghi AM, et al. Evaluation of cerebral metabolism and quantitative electroencephalography after hypothermic circulatory arrest and low-flow cardiopulmonary bypass at different temperatures. *J Thorac Cardiovasc Surg* 1994; 107: 1006–1019.
31. Busija DW and Leffler CW. Hypothermia reduces cerebral metabolic rate and cerebral blood flow in newborn pigs. *Am J Physiol* 1987; 253: H869–H873.
32. Mault JR, Ohtake S, Klingensmith ME, et al. Cerebral metabolism and circulatory arrest: effects of duration and strategies for protection. *Ann Thorac Surg* 1993; 55: 57–64.
33. Skaryak LA, Chai PJ, Kern FH, et al. Blood gas management and degree of cooling: effects on cerebral metabolism before and after circulatory arrest. *J Thorac Cardiovasc Surg* 1995; 110: 1649–1657.
34. Langley SM, Chai PJ, Miller SE, et al. Intermittent perfusion protects the brain during deep hypothermic circulatory arrest. *Ann Thorac Surg* 1999; 68: 4–12.
35. Cavus E, Hoffmann G, Bein B, et al. Cerebral metabolism during deep hypothermic circulatory arrest vs moderate hypothermic selective cerebral perfusion in a piglet model: a microdialysis study. *Paediatr Anaesth* 2009; 19: 770–778.
36. Walther T, Dhein S, Ullmann C, et al. Cerebral protection during controlled hypoperfusion in a piglet model: comparison of moderate (25 degrees C) versus deep (18 degrees C) hypothermia at various flow rates using intraoperative measurements and ex vivo investigation. *Thorac Cardiovasc Surg* 2013; 61: 546–552.
37. Torricelli A, Contini D, Mora AD, et al. Neurophotonic: non-invasive optical techniques for monitoring brain functions. *Funct Neurol* 2014; 29: 223–230.
38. Durduran T and Yodh AG. Diffuse correlation spectroscopy for non-invasive, micro-vascular cerebral blood flow measurement. *Neuroimage* 2014; 85: 5163.
39. Bale G, Elwell CE and Tachtsidis I. From Jobsis to the present day: a review of clinical near-infrared spectroscopy measurements of cerebral cytochrome-c-oxidase. *J Biomed Opt* 2016; 21: 091307.

40. Mavroudis CD, Karlsson M, Ko T, et al. Cerebral mitochondrial dysfunction associated with deep hypothermic circulatory arrest in neonatal swine†. *Eur J Cardiothorac Surg* 2018; 54: 162–168.
41. Stone JG, Young WL, Smith CR, et al. Do standard monitoring sites reflect true brain temperature when profound hypothermia is rapidly induced and reversed? *Anesthesiology* 1995; 82: 344–351.
42. Fuller S, Rajagopalan R, Jarvik GP, et al. J. Maxwell Chamberlain Memorial Paper for congenital heart surgery. Deep hypothermic circulatory arrest does not impair neurodevelopmental outcome in school-age children after infant cardiac surgery. *Ann Thorac Surg* 2010; 90: 1985–1994; discussion 1994–1995.
43. Gaynor JW, Stopp C, Wypij D, et al. Impact of operative and postoperative factors on neurodevelopmental outcomes after cardiac operations. *Ann Thorac Surg* 2016; 102: 843–849.
44. Wang LV and Hsin-I Wu. *Biomedical optics: principles and imaging*. Hoboken, NJ, USA: John Wiley & Sons, Inc., 2012.
45. Durduran T, Choe R, Baker WB, et al. Diffuse optics for tissue monitoring and tomography. *Reports Prog Phys* 2010; 73: 076701.
46. Bigio IJ, Fantini S. *Quantitative Biomedical Optics: Theory, Methods, and Applications*. 1st ed. New York, NY: Cambridge University Press, 2016.
47. Hueber DM, Franceschini MA, Ma HY, et al. Non-invasive and quantitative near-infrared haemoglobin spectrometry in the piglet brain during hypoxic stress, using a frequency-domain multidistance instrument. *Phys Med Biol* 2001; 46: 41–62.
48. Kreis R, Ernst T and Ross BD. Development of the human brain: in vivo quantification of metabolite and water content with proton magnetic resonance spectroscopy. *Magn Reson Med* 1993; 30: 424–437.
49. Jacques SL. Optical properties of biological tissues: a review. *Phys Med Biol* 2013; 58: R37.
50. Fantini S, Hueber D, Franceschini MA, et al. Non-invasive optical monitoring of the newborn piglet brain using continuous-wave and frequency-domain spectroscopy. *Phys Med Biol* 1999; 44: 1543–1563.
51. Boas DA and Yodh AG. Spatially varying dynamical properties of turbid media probed with diffusing temporal light correlation. *J Opt Soc Am A* 1997; 14: 192.
52. Mesquita RC, Durduran T, Yu G, et al. Direct measurement of tissue blood flow and metabolism with diffuse optics. *Philos Trans R Soc A Math Phys Eng Sci* 2011; 369: 4390–4406.
53. Patterson MS, Andersson-Engels S, Wilson BC, et al. Absorption spectroscopy in tissue-simulating materials: a theoretical and experimental study of photon paths. *Appl Opt* 1995; 34: 22.
54. Irwin D, Dong L, Shang Y, et al. Influences of tissue absorption and scattering on diffuse correlation spectroscopy blood flow measurements. *Biomed Opt Exp* 2011; 2: 1969.
55. Kety SS and Schmidt CF. The nitrous oxide method for the quantitative determination of cerebral blood flow in man: theory, procedure and normal values. *J Clin Invest* 1948; 27: 476–483.
56. Schell RM and Cole DJ. Cerebral monitoring: jugular venous oximetry. *Anesth Analg* 2000; 90: 559–566.
57. Kabalin AE, Balenovic T, Valpotic I, et al. The influence of birth mass and age of suckling piglets on erythrocyte parameters. *Vet Arch* 2008; 78: 307–319.
58. Larimer JL. Hemoglobin concentration and oxygen capacity of mammalian blood. 1959.
59. Ito H, Kanno I, Iida H, et al. Arterial fraction of cerebral blood volume in humans measured by positron emission tomography. *Ann Nucl Med* 2001; 15: 111–116.
60. Watzman HM, Kurth CD, Montenegro LM, et al. Arterial and venous contributions to near-infrared cerebral oximetry. *Anesthesiology* 2000; 93: 947–953.
61. Culver JP, Durduran T, Furuya D, et al. Diffuse optical tomography of cerebral blood flow, oxygenation, and metabolism in rat during focal ischemia. *J Cereb Blood Flow Metab* 2003; 23: 911–924.
62. Liu P, Chalak LF and Lu H. Non-invasive assessment of neonatal brain oxygen metabolism: a review of newly available techniques. *Early Hum Dev* 2014; 90: 695–701.
63. van't Hoff MJH. Etudes de dynamique chimique. *Recl des Trav Chim des Pays-Bas* 1884; 3: 333–336.
64. Arrhenius S. *Über die Dissociationswärme und den Einfluss der Temperatur auf den Dissociationsgrad der Elektrolyte*. Leipzig: Wilhelm Engelmann, 1889.
65. Laidler KJ. The development of the Arrhenius equation. *J Chem Educ* 1984; 61: 494.
66. Field J, Fuhrman FA and Martin AW. Effect of temperature on the oxygen consumption of brain tissue. *J Neurophysiol* 1944; 7: 117–126.
67. Chapman AG. Temperature response of oxygen uptake in brain mitochondria from normal and ischemic rats. *Neurochem Int* 1982; 4: 39–47.
68. Michenfelder JD and Milde JH. The effect of profound levels of hypothermia (below 14 °C) on canine cerebral metabolism. *J Cereb Blood Flow Metab* 1992; 12: 877–880.
69. Bland JM and Altman DG. Agreement between methods of measurement with multiple observations per individual. *J Biopharm Stat* 2007; 17: 571–582.
70. Krouwer JS. Why Bland-Altman plots should use  $(Y + X)/2$  when X is a reference method. *Stat Med* 2008; 27: 778–780.
71. Johnson RI, Fox MA, Grayson A, et al. Should we rely on nasopharyngeal temperature during cardiopulmonary bypass? *Perfusion* 2002; 17: 145–151.
72. Engelman R, Baker RA, Likosky DS, et al. The Society of Thoracic Surgeons, The Society of Cardiovascular Anesthesiologists, and The American Society of ExtraCorporeal Technology: clinical practice guidelines for cardiopulmonary bypass – temperature management during cardiopulmonary bypass. *J Cardiothorac Vasc Anesth* 2015; 29: 1104–1113.
73. Bacher A. Effects of body temperature on blood gases. *Intensive Care Med* 2005; 31: 24–27.
74. Toraman F, Evrenkaya S, Senay S, et al. Adjusting oxygen fraction to avoid hyperoxemia during

- cardiopulmonary bypass. *Asian Cardiovasc Thorac Ann* 2007; 15: 303–306.
75. Sasaki T, Boni L, Riemer RK, et al. Cerebral oxygen metabolism during total body flow and antegrade cerebral perfusion at deep and moderate hypothermia. *Artif Organs* 2010; 34: 980–986.
  76. Kern FH, Schell RM and Greeley WJ. Cerebral monitoring during cardiopulmonary bypass in children. *J Neurosurg Anesthesiol* 1993; 5: 213–217.
  77. Abdul-Khaliq H, Troitsch D, Berger F, et al. Regional transcranial oximetry with near infrared spectroscopy (NIRS) in comparison with measuring oxygen saturation in the jugular bulb in infants and children for monitoring cerebral oxygenation. *Biomed Tech Eng* 2000; 45: 328–332.
  78. Daubeney PEF, Pilkington SN, Janke E, et al. Cerebral oxygenation measured by near-infrared spectroscopy: comparison with jugular bulb oximetry. *Ann Thorac Surg* 1996; 61: 930–934.
  79. Nagdyman N, Fleck T, Schubert S, et al. Comparison between cerebral tissue oxygenation index measured by near-infrared spectroscopy and venous jugular bulb saturation in children. *Intensive Care Med* 2005; 31: 846–850.
  80. Rudinsky BF and Meadow WL. Internal jugular venous oxygen saturation does not reflect sagittal sinus oxygen saturation in piglets. *Neonatology* 1991; 59: 322–328.
  81. Hansen NB, Brubakk A-M, Bratlid D, et al. The effects of variations in Paco<sub>2</sub> on brain blood flow and cardiac output in the newborn piglet. *Pediatr Res* 1984; 18: 1132–1136.
  82. Laptook AR, Shalak L and Corbett RJT. Differences in brain temperature and cerebral blood flow during selective head versus whole-body cooling. *Pediatrics* 2001; 108: 1103–1110.
  83. Scheers G, Zaitseva T, Schultz S, et al. Brain oxygenation and metabolism during selective cerebral perfusion in neonates. *Eur J Cardio thorac Surg* 2006; 29: 168–174.
  84. Gagnon L, Desjardins M, Jehanne-Lacasse J, et al. Investigation of diffuse correlation spectroscopy in multi-layered media including the human head. *Opt Exp* 2008; 16: 15514–15530.
  85. Mesquita RC, Schenkel SS, Minkoff DL, et al. Influence of probe pressure on the diffuse correlation spectroscopy blood flow signal: extra-cerebral contributions. *Biomed Opt Exp* 2013; 4: 978.
  86. Baker WB, Parthasarathy AB, Ko TS, et al. Pressure modulation algorithm to separate cerebral hemodynamic signals from extracerebral artifacts. *Neurophotonics* 2015; 2: 035004.
  87. Conrad MS, Dilger RN and Johnson RW. Brain growth of the domestic pig (*Sus scrofa*) from 2 to 24 weeks of age: a longitudinal MRI study. *Dev Neurosci* 2012; 34: 291–298.
  88. Semenas E, Nozari A and Wiklund L. Sex differences in cardiac injury after severe haemorrhage and ventricular fibrillation in pigs. *Resuscitation* 2010; 81: 1718–1722.
  89. Armstead WM, Kiessling JW, Kofke WA, et al. Impaired cerebral blood flow autoregulation during posttraumatic arterial hypotension after fluid percussion brain injury is prevented by phenylephrine in female but exacerbated in male piglets by extracellular signal-related kinase mitogen-activated prot. *Crit Care Med* 2010; 38: 1868–1874.
  90. Takayama JI, Teng W, Uyemoto J, et al. Body temperature of newborns: what is normal? *Clin Pediatr* 2000; 39: 503–510.
  91. Anand KJS and Hickey PR. Halothane–morphine compared with high-dose sufentanil for anesthesia and postoperative analgesia in neonatal cardiac surgery. *N Engl J Med* 1992; 326: 1–9.
  92. Enomoto S, Hindman BJ, Dexter F, et al. Rapid rewarming causes an increase in the cerebral metabolic rate for oxygen that is temporarily unmatched by cerebral blood flow. A study during cardiopulmonary bypass in rabbits. *Anesthesiology* 1996; 84: 1392–400.
  93. Condò SG, Corda M, Sanna MT, et al. Molecular basis of low-temperature sensitivity in pig hemoglobins. *Eur J Biochem* 1992; 209: 773–776.
  94. Willford DC and Hill EP. Modest effect of temperature on the porcine oxygen dissociation curve. *Respir Physiol* 1986; 64: 113–123.
  95. Henriksen OM, Vestergaard MB, Lindberg U, et al. Interindividual and regional relationship between cerebral blood flow and glucose metabolism in the resting brain. *J Appl Physiol* 2018; 125: 1080–1089.
  96. Ito H, Ibaraki M, Kanno I, et al. Changes in cerebral blood flow and cerebral oxygen metabolism during neural activation measured by positron emission tomography: comparison with blood oxygenation level-dependent contrast measured by functional magnetic resonance imaging. *J Cereb Blood Flow Metab* 2005; 25: 371–377.
  97. Rodgers ZB, Detre JA and Wehrli FW. MRI-based methods for quantification of the cerebral metabolic rate of oxygen. *J Cereb Blood Flow Metab* 2016; 36: 1165–1185.
  98. Sundar LK, Muzik O, Rischka L, et al. Towards quantitative [18F]FDG-PET/MRI of the brain: automated MR-driven calculation of an image-derived input function for the non-invasive determination of cerebral glucose metabolic rates. *J Cereb Blood Flow Metab*. Epub ahead of print 23 May 2018; DOI: 10.1177/0271678X18776820.
  99. Gaynor JW, Nicolson SC, Jarvik GP, et al. Increasing duration of deep hypothermic circulatory arrest is associated with an increased incidence of postoperative electroencephalographic seizures. *J Thorac Cardiovasc Surg* 2005; 130: 1278–1286.
  100. Shankaran S, Laptook AR, Ehrenkranz RA, et al. Whole-body hypothermia for neonates with hypoxic-ischemic encephalopathy. *N Engl J Med* 2005; 353: 1574–1584.
  101. Laptook AR, Shankaran S, Tyson JE, et al. Effect of therapeutic hypothermia initiated after 6 hours of age on death or disability among newborns with hypoxic-ischemic encephalopathy a randomized clinical trial. *JAMA* 2017; 318: 1550–1560.
  102. Rutherford M, Ramenghi LA, Edwards AD, et al. Assessment of brain tissue injury after moderate hypothermia in neonates with hypoxic-ischaemic encephalopathy: a nested substudy of a randomised controlled trial. *Lancet Neurol* 2010; 9: 39–45.

103. Edwards AD, Brocklehurst P, Gunn AJ, et al. Neurological outcomes at 18 months of age after moderate hypothermia for perinatal hypoxic ischaemic encephalopathy: synthesis and meta-analysis of trial data. *BMJ* 2010; 340: 409.
104. Massaro AN, Govindan RB, Vezina G, et al. Impaired cerebral autoregulation and brain injury in newborns with hypoxic-ischemic encephalopathy treated with hypothermia. *J Neurophysiol* 2015; 114: 818–824.
105. Dehaes M, Aggarwal A, Lin P-Y, et al. Cerebral oxygen metabolism in neonatal hypoxic ischemic encephalopathy during and after therapeutic hypothermia. *J Cereb Blood Flow Metab* 2014; 34: 87–94.